LETTER

doi:10.1038/nature10204

Quantum quench of Kondo correlations in optical absorption

C. Latta[1], F. Haupt[1], M. Hanl[2], A. Weichselbaum[2], M. Claassen[1], W. Wuester[1], P. Fallahi[1], S. Faelt[1], L. Glazman[3], J. von Delft[2], H. E. Türeci[1,4] & A. Imamoglu[1]

The interaction between a single confined spin and the spins of an electron reservoir leads to one of the most remarkable phenomena of many-body physics—the Kondo effect[1,2]. Electronic transport measurements on single artificial atoms, or quantum dots, have made it possible to study the effect in great detail[3–5]. Here we report optical measurements on a single semiconductor quantum dot tunnel-coupled to a degenerate electron gas which show that absorption of a single photon leads to an abrupt change in the system Hamiltonian and a quantum quench of Kondo correlations. By inferring the characteristic power-law exponents from the experimental absorption line shapes, we find a unique signature of the quench in the form of an Anderson orthogonality catastrophe[6,7], induced by a vanishing overlap between the initial and final many-body wavefunctions. We show that the power-law exponent that determines the degree of orthogonality can be tuned using an external magnetic field[8], which unequivocally demonstrates that the observed absorption line shape originates from Kondo correlations. Our experiments demonstrate that optical measurements on single artificial atoms offer new perspectives on many-body phenomena previously studied using transport spectroscopy only.

Optical spectroscopy of single quantum dots has demonstrated its potential for applications in quantum information processing, particularly in the realization of single- and entangled-photon sources[9,10], coherent spin qubits[11,12] and a spin–photon interface[13,14]. Although recent experiments have established this system as a new model for solid-state quantum optics, all of the striking experimental observations made so far can be understood within the framework of single- or few-particle physics enriched by perturbative coupling to reservoirs involving phonons, a degenerate electron gas[15–17] or nuclear spins[18,19].

We present differential transmission experiments[20] on single, charge-tunable quantum dots that reveal optical signatures of the Kondo effect. By contrast with prior experiments[17,21], the tunnel coupling between the quantum dot and a nearby degenerate electron gas, which we refer to as the fermionic reservoir, is engineered to be so strong that the resulting exchange interactions cannot be treated using a perturbative system–reservoir theory: in the initial state, the 'system'—quantum dot spin—is maximally entangled with the fermionic reservoir, forming a singlet. Various settings have been proposed for finding optical signatures of Kondo physics[8,22–25]; our work is most closely related to the theoretical investigation of refs 8, 25.

The feature that differentiates our results from all prior transport-based investigations of the Kondo effect[3–5] is the realization of a quantum quench of the local Hamiltonian; in our experiments, photon absorption abruptly turns off the exchange interaction between the quantum dot electron and the fermionic reservoir, leading to the destruction of the correlated dot–reservoir singlet that otherwise acts as a local scattering potential for all reservoir electrons. The overlap between N-electron fermionic reservoir states with and without a local scattering potential scales as $N^{-\alpha}$, with $\alpha > 0$ (refs 6, 7). This reduced overlap, called an Anderson orthogonality catastrophe (AOC), leads to a power-law tail in absorption if the scattering potential is turned on or off by photon absorption. Here we determine the AOC-induced power-law exponents in the absorption line shape that uniquely characterize the quench of Kondo correlations. Moreover, by tuning the applied laser frequency, we observe both the perturbative and the non-perturbative regimes of the Kondo effect in one absorption line shape, without having to change the fermionic reservoir (electron) temperature, T_{FR}. The AOC after a Kondo quench can, in principle, also be probed by core-level X-ray absorption spectroscopy of suitable bulk materials[26], but optical studies of quantum dots offer higher resolution and a tunable local Hamiltonian.

The quantum dot sample we study is shown schematically in Fig. 1a: a gate voltage, V_g, applied between a top Schottky gate and the degenerate electron gas, allows us to tune the charging state of the quantum dot[27]. Figure 1b shows the photoluminescence spectrum of a particular quantum dot (dot 1), as a function of V_g, where different discrete 'charging plateaux' are clearly observable. The dependence of the photoluminescence energy on the quantum dot charging state originates from a Coulomb renormalization of the optical transition energy. In addition to photoluminescence lines (for example X^0) associated with a fixed charging state (for example neutral) of the quantum dot, we also observe spatially indirect transitions with a strong dependence on V_g (refs 8, 17; see Fig. 1b, red arrow).

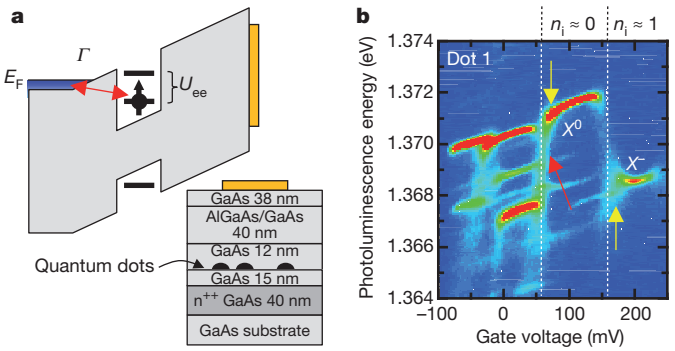

Figure 1 | Single quantum dot strongly coupled to a fermionic reservoir. **a**, Band structure of the device. The quantum dots are separated by a 15-nm tunnel barrier from an n^{++}-doped GaAs layer (fermionic reservoir). A voltage, V_g, applied between the electron gas and a semi-transparent NiCr gate on the sample surface controls the relative value of the quantum dot single-particle energy levels with respect to the Fermi energy, E_F. **b**, Low-temperature (4 K) photoluminescence spectrum of a single quantum dot (dot 1) as a function of V_g; n_i denotes the initial state electron occupancy of the quantum dot. The interaction of the quantum dot electron with the Fermi sea leads to a broadening of the photoluminescence lines at the plateau edges (yellow arrows) and indirect recombinations of a quantum dot hole and a Fermi sea electron (red arrow). Indirect transitions are identified by the stronger V_g dependence of the transition energy, compared with that for direct transitions. A detailed discussion of the origin of various photoluminescence lines can be found in ref. 17.

[1]Institute of Quantum Electronics, ETH-Zürich, CH-8093 Zürich, Switzerland. [2]Arnold Sommerfeld Center for Theoretical Physics, Ludwig-Maximilians-Universität München, D-80333 München, Germany. [3]Sloane Physics Laboratory, Yale University, New Haven, Connecticut 06520, USA. [4]Department of Electrical Engineering, Princeton University, Princeton, New Jersey 08544, USA.

In this Letter, we focus on the X^- plateau, for which the quantum dot carries the charge of a single electron and the influence of the fermionic reservoir on the quantum dot photoluminescence dispersion and linewidth is strongest. The X^- optical transition couples the initial configuration, containing on average one electron in the quantum dot, to a final configuration, containing on average two electrons and a valence-band hole (a negatively charged trion). This transition can be described within the framework of an excitonic Anderson model[8,25] (EAM), depicted schematically in Fig. 2c (and described explicitly in Supplementary Information). It is parameterized by the energy, ε, of the quantum dot electron level with respect to the Fermi level; the on-site Coulomb repulsion, U_{ee}; the tunnelling rate, Γ, between quantum dot and fermionic reservoir; the half-bandwidth, D, of the fermionic reservoir; and the electron–hole Coulomb attraction, U_{eh}. The last is relevant only in the final configuration, where it effectively lowers the electron level energy to $\varepsilon - U_{eh}$, thus ensuring the double occupancy of the electron level. An estimate from the photoluminescence data in Fig. 1b yields $U_{eh} \approx U_{ee} + 4$ meV.

The inset of Fig. 2a shows high-resolution laser absorption spectroscopy on dot 1 across the X^- single-electron charging plateau

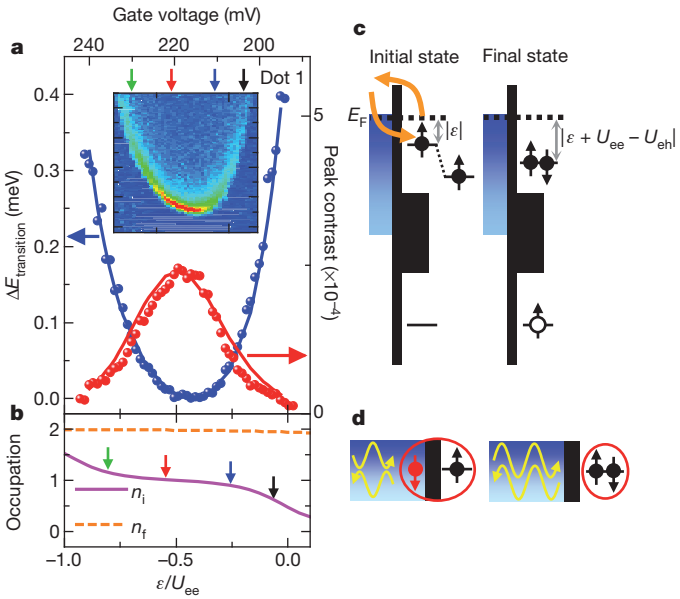

Figure 2 | Gate voltage dependence of the peak absorption strength. **a**, Experimental data (symbols) for the ε dependence of the shift in the resonance energy, $\Delta E_{transition}$ (blue, left axis), and the absorption contrast (red, right axis) are well reproduced by NRG calculations (solid lines) for the following parameters: $U_{ee} = 7.5$ meV, $\Gamma = 0.7$ meV, $D = 3.5$ meV, $U_{eh} = 11$ meV, $T_{FR} = 180$ mK. Inset, absorption on the negatively charged exciton X^- transition of dot 1 as a function of the gate voltage, measured at $T_{FR} = 180$ mK. **b**, NRG results for the respective occupancies, n_i and n_f, of the quantum dot electron level in the initial and final ground states. **c**, Energy renormalization process: the initial configuration (left) features a single electron in the quantum dot, whose energy is lowered by virtual tunnelling between the dot and the fermionic reservoir. Because virtual excitations with energy ΔE contribute a shift proportional to $-\Gamma/\Delta E$, the total shift (involving a sum over all possible values of ΔE), is strongest near the edges of the X^- plateau. Towards the right-hand edge (ε near zero), the dominant contribution comes from virtual tunnelling of the quantum dot electron into the fermionic reservoir (as depicted); towards the left-hand edge (ε near $-U_{ee}$), it comes from virtual tunnelling of a fermionic reservoir electron into the quantum dot (not depicted). In the final configuration (right), the quantum dot contains two electrons and a hole. The electron–hole Coulomb attraction, U_{eh}, effectively lowers the quantum dot electron level energy to $\varepsilon - U_{eh}$. This raises the energy cost, ΔE, for virtual excitations by $U_{eh} - U_{ee}$ (which is $\gg \Gamma$), such that the final-state energy renormalization is negligible. The renormalization of the transition energy, probed by a weak laser, is thus mainly due to initial-state energy renormalization. **d**, Anderson orthogonality: the Kondo cloud (left-hand diagram) and local singlet (right-hand diagram) of the initial and final configurations produce strong or weak scattering phase shifts, respectively.

(Supplementary Information). Here we parameterize V_g in terms of ε, normalized and shifted such that $\varepsilon = -U_{ee}/2$ for the gate voltage at which the absorption contrast is maximal. Instead of the usual linear d.c. Stark shift of the absorption peak that is characteristic of charge-tunable quantum dots, we find a strongly nonlinear, ε-dependent shift of the X^- transition energy[15,17], which measures the energy difference between the final and initial ground states. As shown in Fig. 2c, this energy shift arises from a renormalization of the initial state energy[28] due to virtual tunnelling between the singly occupied quantum dot and the fermionic reservoir (analogous to the Lamb shift of atomic ground states). The final trion state energy, on the other hand, is hardly affected by virtual tunnelling processes, owing to $U_{eh} - U_{ee}$ being large. This renormalization-induced redshift of the initial state is strongest at the plateau edges and leads to an ε-dependent blueshift of the optical resonance frequency. The latter can be used to determine the EAM parameters for dot 1: $U_{ee} = 7.5$ meV, $\Gamma = 0.7$ meV and $D = 3.5$ meV. Numerical renormalization group (NRG) calculations for the transition energy (Fig. 2a, blue line) give excellent agreement with the experimental data (blue symbols).

We now consider the detailed form of the absorption line shape, $A(\nu)$, as function of the detuning, ν, between the applied laser frequency and the transition threshold. Figure 3a shows, on a log–log scale, the blue ($\nu > 0$) tail of $A(\nu)$ for dot 1, for the four values of gate voltage indicated by arrows in the inset of Fig. 2a. The inset of Fig. 3a compares the full, un-normalized absorption line shapes for the same gate voltages on a linear scale; the red ($\nu < 0$) absorption tail allows us to determine the temperature of the fermionic reservoir to be

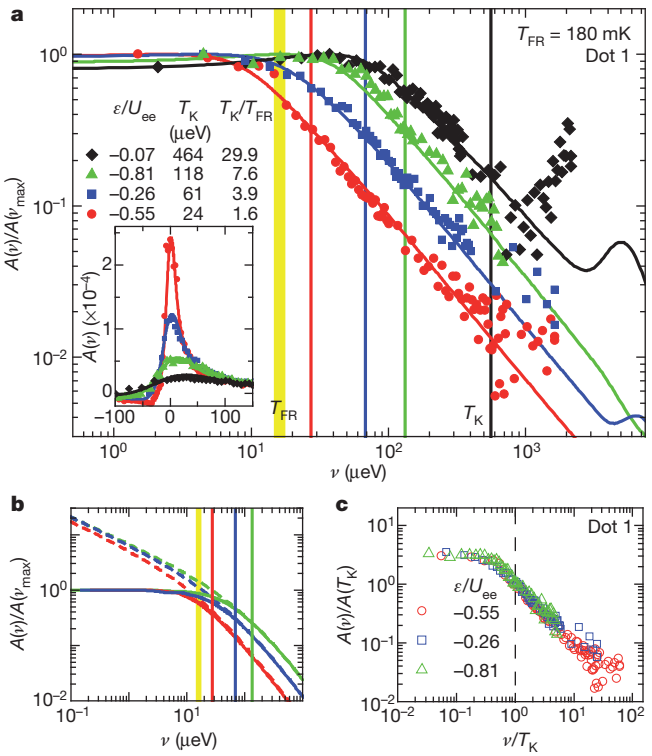

Figure 3 | The absorption line shape $A(\nu)$. **a**, Blue tail of $A(\nu)/A(\nu_{max})$ for dot 1, plotted versus the laser detuning, ν, on a log–log scale. Here ν_{max} is the threshold frequency for which the absorption strength is maximal. The experimental data were measured at an electron temperature of $T_{FR} = 180$ mK for the four values of gate voltage, ε, indicated by arrows in Fig. 2a; the corresponding Kondo temperatures, $T_K(\varepsilon)$, are indicated by vertical lines in matching colours. The yellow line indicates T_{FR}. NRG results (solid lines), obtained using the parameters from the fit in Fig. 2a, are in remarkable agreement with experiment. Inset, the measured full (un-normalized) absorption line shape for the same ε values, plotted on a linear scale. **b**, NRG results for $T = T_{FR}$ (solid lines) and $T_{FR} = 0$ (dashed lines); the latter show the $\nu^{-0.5}$ behaviour expected in the strong-coupling regime, $T_{FR} \ll \nu \ll T_K$. **c**, The rescaled line shape, $A(\nu)/A(T_K)$, versus ν/T_K shows a universal scaling collapse characteristic of Kondo physics.

$T_{FR} = 180$ mK, equivalent to 15.6 μeV (Supplementary Information). The strong variation of the peak absorption strength and width shown in the inset of Fig. 3a is a consequence of the exponential dependence of the Kondo temperature on the gate voltage ε:

$$T_K(\varepsilon) = \sqrt{\Gamma D}\exp\left[-\left(1-\left(\frac{2\varepsilon}{U_{ee}}+1\right)^2\right)\frac{\pi U_{ee}}{8\Gamma}\right] \quad (1)$$

For dot 1, T_K varies between 24 and 118 μeV; we emphasize that even though $T_K = 464$ μeV for the black curve (Fig. 3a, inset), the dot–reservoir system is no longer in the local moment regime for this gate voltage. All line shapes carry the signatures of an optical interference effect induced by the sample structure (causing some line shapes to become negative for small red detunings), and of independently measured fluctuations in gate voltage; both effects have been taken into account in the calculated line shapes (Supplementary Information). Calculating the line shapes using NRG (solid lines) without any further fit parameters, we find remarkable agreement with experiment for all four line shapes shown in Fig. 3a, demonstrating the validity of the EAM[8] for the coupled dot–reservoir system.

For blue detunings satisfying $\nu > \max(T_{FR}, T_K)$, a perturbative description for $A(\nu)$ is possible. The frequency scale for which the perturbative $\sim\nu^{-1}$ dependence in Fig. 3a sets in and the peak absorption contrast itself both strongly depend on gate voltage. Remarkably, for gate voltages such that the initial ground state is a Kondo singlet, this dependence is such that it permits a scaling collapse: Fig. 3c shows the normalized absorption line shape, $A(\nu)/A(T_K(\varepsilon))$, as a function of ν/T_K for the red, green and blue curves of Fig. 3a (but omitting the black curve, which is in the mixed valence regime). We find that all three curves collapse to a universal scaling function of ν/T_K, as expected[8] for the regime $T_{FR} \ll \nu \ll U_{ee}$. Thus, the ε dependence of the crossover scale is captured by equation (1) for T_K; this observation is unequivocal proof that the Kondo effect is indeed present in our system.

In the limit $T_{FR} < \nu < T_K$, a perturbative description of the line shape is no longer valid. In the initial configuration, the exchange interaction between the quantum dot and the fermionic reservoir induces a 'Kondo screening cloud' that forms a singlet with the quantum dot spin. This acts as a scattering potential that induces strong phase shifts for those low-energy fermionic excitations whose energies differ from the Fermi level by T_K or less. In the final configuration after photon absorption, the quantum dot has two electrons in a local singlet state. Therefore, the Kondo screening cloud, and the scattering potential that it constitutes for reservoir electrons, disappears in the long-time limit: the corresponding ground-state wavefunction is a tensor product of the local singlet and free electronic states, with only weak phase shifts. Because the initial and final fermionic reservoir phase shifts differ (as depicted schematically in Fig. 2d), the fermionic reservoir does not remain a spectator during the X^- transition; instead, the transition matrix element between the ground states of the initial and final configurations is vanishingly small. This leads to an AOC that manifests itself by transforming a delta-function resonance (of an uncoupled quantum dot) into a power-law singularity[6] of the form $\nu^{-\eta}$, where the exponent η characterizes the extent of the AOC. For $T_{FR} \ll \nu \ll T_K$, the absorption line shape of the X^- transition is expected to show an analogous power-law singularity. The exponent η is predicted[8,25] to range between 0 and 0.5 (assuming no magnetic field), with $\eta \approx 0.5$ being characteristic for a Kondo-correlated initial state and an uncorrelated final state. This line shape modification is a consequence of a redistribution of the optical oscillator strength, associated with the fact that the fermionic reservoir wavefunction in the Kondo-correlated initial state has finite overlap with a range of final states consisting of electron–hole pair excitations out of a non-interacting fermionic reservoir.

If $T_{FR} \ll T_K$ and the optical detuning is reduced below T_K, the line shape is predicted to cross over smoothly from the perturbative $1/\nu$ tail to the strong-coupling $1/\nu^{0.5}$ power law just discussed. This crossover is illustrated in Fig. 3b (dashed lines) by NRG calculations, performed at $T_{FR} = 0$ for the three ε values of Fig. 3c: Remarkably, despite drastic differences in the $\nu > T_K$ tails due to different values of $T_K(\varepsilon)$, all three line shapes show similar power-law exponents, of around $\eta \approx 0.5$, for $\nu \ll T_K$. For non-zero temperature, however, the $1/\nu^{0.5}$ power law is cut off and saturates once ν decreases past T_{FR} (Fig. 3b, solid lines), because of thermal averaging over initial states with excitation energies $\leq T_{FR}$.

A direct extraction of the $1/\nu^{0.5}$ power law from the measured data is difficult owing to the small accessible experimental window, $T_{FR} < \nu < T_K$. Nevertheless, we are able to determine the power-law exponent accurately for a more strongly coupled quantum dot (dot 2) by using the fact that the detailed form of the line shape sensitively depends on the exponent η, which can be tuned using an external magnetic field[8]. This tunability arises because the magnetic field, B_{ext}, changes the initial dot occupancies, favouring spin up over spin down, and hence affects the overlap between the initial and final states of the transition (Supplementary Information). Figure 4a shows the $B_{ext} = 0$ absorption line shape for dot 2 with parameters $U_{ee} = 7.5$ meV, $\Gamma = 1$ meV, $D = 6.5$ meV and $U_{eh} = (3/2)U_{ee}$, measured at $\varepsilon/U_{ee} = -0.43$ (where $T_K = 140$ μeV) and $T_{FR} = 15.6$ μeV. An attempt to obtain a fit to the experimental absorption line shape using a perturbative formula[8]

$$A(\nu) \propto \frac{\nu/T_{FR}}{1-e^{-\nu/T_{FR}}}\,\frac{\gamma}{\nu^2+\gamma^2/4}$$

where $\gamma \leq T_{FR}$ denotes a phenomenological relaxation rate, fails markedly for dot 2 (Fig. 4a, red curve). By striking contrast, Fig. 4b shows that an excellent fit is obtained for a weakly coupled dot (dot 3; Supplementary Information).

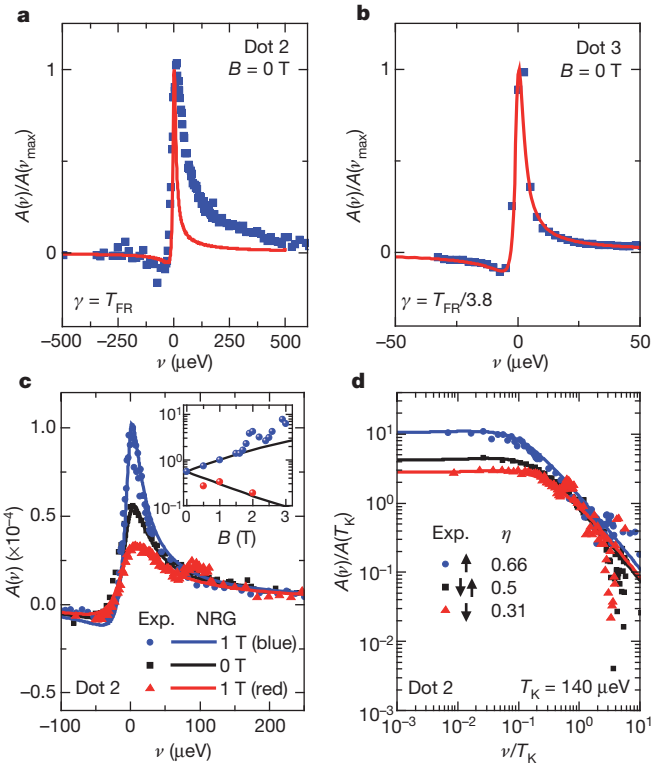

Figure 4 | Magnetic field dependence of the absorption. **a**, The absorption line shape of dot 2 for $B = 0$ (symbols) cannot be fit by the perturbative formula (red line) given in the text. **b**, By contrast, for dot 3 such a fit works well. **c**, Absorption line shapes for dot 2, at $B_{ext} = 0$ and 1 T, for the blue–red trion transition. The magnetic field changes the strength of the AOC and the line shape. The small peak that appears at $\nu \approx 80$ μeV in the red trion absorption is due to incomplete suppression of the laser polarization that couples to the blue trion transition. Inset, the peak absorption contrast shows good agreement with the NRG calculations for $B_{ext} \leq 1.5$ T. **d**, Normalized absorption line shape for dot 2 in a log–log plot. These measurements pin the value of $\eta(B_{ext} = 0)$ to ~0.5, which is a direct signature of a Kondo singlet in the absorption line shape. In addition, they demonstrate the tunability of an orthogonality exponent.

Figure 4c shows the magnetic field dependence of the line shape of dot 2, measured in Faraday geometry, where quantum dot optical selection rules[13] ensure that by choosing right- or left-handed circular polarization of the laser field, it is possible to probe selectively the blue or, respectively, red trion transition that couples exclusively to the spin-up or, respectively, spin-down initial state. In comparison with the $B_{ext} = 0$ (Fig. 4c, black squares) results, the absorption line shapes for the blue (Fig. 4c; blue dots) and red (Fig. 4c; red triangles) trion transitions at $B_{ext} = 1$ T exhibit two striking features: the peak contrast increases (blue) or decreases (red) by a factor of ~2, and the area under the absorption curve increases (blue) or decreases (red) by less than 20%. These observations indicate that the change in the $B_{ext} \leq 1.5$ T line shapes is predominantly due to a line narrowing associated with an increase in the AOC power-law exponent, η, of the blue trion transition and a line broadening associated with a decrease in η for the red trion transition. To quantify the field-induced change in η, we plot in Fig. 4d the corresponding normalized line shapes, $A(v)/A(T_K)$, as functions of v/T_K in a log–log plot, together with the corresponding NRG results (solid lines): the latter yield $\eta = 0.5$ at $B_{ext} = 0$ and $\eta = 0.31$ (red trion) and $\eta = 0.66$ (blue trion) at $B_{ext} = 1$ T, proving the remarkable sensitivity of the measured line shapes to the AOC-determined power-law exponents. By contrast with Fig. 3c, the line shapes in Fig. 4d do not show a scaling collapse. We emphasize that qualitatively similar features are observed for all field values $B_{ext} \leq 1.5$ T; for $B_{ext} > 1.5$ T, the blue trion absorption contrast has oscillations (Fig. 4c, inset), most probably stemming from the modification of the fermionic reservoir density of states at high fields in Faraday geometry.

The area under the (un-normalized) absorption line shape is proportional to the initial occupancy, $n_\uparrow$ or $n_\downarrow$, of the spin-up or, respectively, spin-down state. The small (≤20%) field-induced change in the measured areas in Fig. 4c implies a small magnetization, $m = (n_\uparrow - n_\downarrow)/2 \approx 0.16$ (Supplementary Information). By contrast, the corresponding magnetization for a free spin would have been $m = 0.40$. This measurement confirms that the static spin susceptibility of the initial configuration is substantially reduced relative to that of a free spin, providing yet another optical signature of the Kondo screening.

The remarkable agreement between our experimental data depicted in Figs 2–4 and the NRG calculations demonstrates Kondo correlations between a quantum dot electron and the electrons in a fermionic reservoir. The optical probe of these correlations unequivocally shows the signatures of Anderson orthogonality physics associated with the quantum quench of Kondo correlations, with field-tunable power-law exponents. Our experiments establish the potential of single, optically active quantum dots in investigating many-body physics. In addition, they pave the way for a new class of quantum optics experiments in which the influence of the simultaneous presence of non-perturbative cavity or laser coupling and Kondo correlations on electric field and photon correlations could be investigated.

METHODS SUMMARY

The InGaAs quantum dots studied in this work were grown by molecular beam epitaxy; the quantum dot layer was separated by a nominally 15-nm-thick GaAs tunnel barrier from a back gate consisting of a 40-nm-thick n^{++}-doped GaAs layer. This back gate serves as an electron reservoir. The distance from the quantum dot layer to the sample surface was 90 nm. A voltage applied between a 5-nm-thick NiCr top gate and the n^{++} GaAs back gate allows for discrete charging of the quantum dots. The sample was placed inside a fibre-based confocal microscope embedded in a dilution refrigerator with a base temperature of 20 mK in the mixing chamber. The objective was mounted on a stack of low-temperature x–y–z positioners. The cryostat was equipped with a 7-T magnet. The absorption experiments were performed by focusing on a single quantum dot a power- and frequency-stabilized, single-mode tunable laser with an intensity of 15 nW. The objective had a numerical aperture of 0.6, yielding a diffraction-limited spot size. The change in transmission through the sample was recorded using a silicon photodiode. To increase the signal-to-noise ratio, a lock-in technique was used whereby the gate voltage was modulated at 187.195 Hz with a modulation amplitude of 50 mV.

The calculations were carried out using the NRG. The continuous energy spectrum of the Fermi reservoir was logarithmically discretized and mapped onto a semi-infinite chain with exponentially decaying hopping amplitudes. In each iteration, a new site was added to the chain, which corresponds to including ever lower energy scales of the system. By combining NRG data from all iterations, it was possible to construct a complete set of approximate many-body eigenstates of the full Hamiltonian, which could be used to calculate the physical quantities using the full-density-matrix NRG (Supplementary Information).

Received 1 January; accepted 16 May 2011.

1. Kondo, J. Resistance minimum in dilute magnetic alloys. *Prog. Theor. Phys.* **32,** 37–49 (1964).
2. Kouwenhoven, L. P. & Glazman, L. Revival of the Kondo effect. *Phys. World* **14,** 33–38 (January 2001).
3. Goldhaber-Gordon, D. *et al.* Kondo effect in a single-electron transistor. *Nature* **391,** 156–159 (1998).
4. Cronenwett, S. M., Oosterkamp, T. H. & Kouwenhoven, L. P. A tunable Kondo effect in quantum dots. *Science* **281,** 540–544 (1998).
5. van der Wiel, W. G. *et al.* The Kondo effect in the unitary limit. *Science* **289,** 2105–2108 (2000).
6. Mahan, G. *Many-Particle Physics* 612–621 (Kluwer, 2000).
7. Anderson, P. W. Infrared catastrophe in Fermi gases with local scattering potentials. *Phys. Rev. Lett.* **18,** 1049–1051 (1967).
8. Türeci, H. E. *et al.* Many-body dynamics of exciton creation in a quantum dot by optical absorption: a quantum quench towards Kondo correlations. *Phys. Rev. Lett.* **106,** 107402 (2011).
9. Michler, P. *et al.* A quantum dot single-photon turnstile device. *Science* **290,** 2282–2285 (2000).
10. Dousse, A. *et al.* Ultrabright source of entangled photon pairs. *Nature* **466,** 217–220 (2010).
11. Press, D., Ladd, T. D., Zhang, B. & Yamamoto, Y. Complete quantum control of a single quantum dot spin using ultrafast optical pulses. *Nature* **456,** 218–221 (2008).
12. Kim, D. *et al.* Ultrafast optical control of entanglement between two quantum-dot spins. *Nature Phys.* **7,** 223–229 (2011).
13. Yilmaz, S. T., Fallahi, P. & Imamoglu, A. Quantum-dot-spin single-photon interface. *Phys. Rev. Lett.* **105,** 033601 (2010).
14. Claassen, M., Türeci, H. & Imamoglu, A. Solid-state spin-photon quantum interface without spin-orbit coupling. *Phys. Rev. Lett.* **104,** 177403 (2010).
15. Dalgarno, P. A. *et al.* Optically induced hybridization of a quantum dot state with a filled continuum. *Phys. Rev. Lett.* **100,** 176801 (2008).
16. Hilario, L. M. L. & Aligia, A. A. Photoluminescence of a quantum dot hybridized with a continuum of extended states. *Phys. Rev. Lett.* **103,** 156802 (2009).
17. Kleemans, N. A. J. M. *et al.* Many-body exciton states in self-assembled quantum dots coupled to a Fermi sea. *Nature Phys.* **6,** 534–538 (2010).
18. Latta, C. *et al.* Confluence of resonant laser excitation and bidirectional quantum-dot nuclear-spin polarization. *Nature Phys.* **5,** 758–763 (2009).
19. Xu, X. *et al.* Optically controlled locking of the nuclear field via coherent dark-state spectroscopy. *Nature* **459,** 1105–1109 (2009).
20. Högele, A. *et al.* Voltage-controlled optics of a quantum dot. *Phys. Rev. Lett.* **93,** 217401 (2004).
21. Atatüre, M. *et al.* Quantum-dot spin-state preparation with near-unity fidelity. *Science* **312,** 551–553 (2006).
22. Shahbazyan, T. V., Perakis, I. E. & Raikh, M. E. Spin correlations in nonlinear optical response: light-induced Kondo effect. *Phys. Rev. Lett.* **84,** 5896–5899 (2000).
23. Kikoin, K. & Avishai, Y. Many-particle resonances in excited states of semiconductor quantum dots. *Phys. Rev. B* **62,** 4647–4655 (2000).
24. Govorov, A. O., Karrai, K. & Warburton, R. J. Kondo excitons in self-assembled quantum dots. *Phys. Rev. B* **67,** 241307(R) (2003).
25. Helmes, R. W., Sindel, M., Borda, L. & von Delft, J. Absorption and emission in quantum dots: Fermi surface effects of Anderson excitons. *Phys. Rev. B* **72,** 125301 (2005).
26. Gunnarsson, O. & Schönhammer, K. Electron spectroscopies for Ce compounds in the impurity model. *Phys. Rev. B* **28,** 4315–4341 (1983).
27. Warburton, R. J. *et al.* Optical emission from a charge-tunable quantum ring. *Nature* **405,** 926–929 (2000).
28. Anderson, P. W. Localized magnetic states in metals. *Phys. Rev.* **124,** 41–53 (1961).

Supplementary Information is linked to the online version of the paper at www.nature.com/nature.

Acknowledgements This work was supported by Swiss NSF under grant no. 200021-121757 and an ERC Advanced Investigator Grant (A.I.). J.v.D. acknowledges support from the DFG (SFB631, SFB-TR12, De730/3-2, De730/4-1), the Cluster of Excellence 'Nanosystems Initiative Munich'. H.E.T. acknowledges support from the Swiss NSF under grant no. PP00P2-123519/1. L.G. acknowledges support from NSF DMR under grant no. 0906498.

Author Contributions C.L., F.H., W.W. and P.F. carried out the experiments. M.H. and A.W. performed the numerical analysis. The samples were grown by S.F. C.L. and A.I. planned the experiment. H.E.T., M.C., L.G., A.I. and J.v.D. developed the theoretical framework. C.L., J.v.D. and A.I. supervised the project, carried out the analysis of the data and wrote the manuscript.

Author Information Reprints and permissions information is available at www.nature.com/reprints. The authors declare no competing financial interests. Readers are welcome to comment on the online version of this article at www.nature.com/nature. Correspondence and requests for materials should be addressed to C.L. (clatta@phys.ethz.ch) or A.I. (imamoglu@phys.ethz.ch).